Combustion performances of premixed ammonia/hydrogen/air laminar and swirling flames for a wide range of equivalence ratios

S. Mashruk, S.E. Zitouni, Pierre Brequigny, C. Mounaim-Rousselle, A. Valera-Medina

Combustion performances of premixed ammonia/hydrogen/air laminar and swirling flames for a wide range of equivalence ratios

Mashruk S[1]*, Zitouni SE[2]**, Brequigny P[2], Mounaim-Rousselle C[2], Valera-Medina A[1]

[1]College of Physical Sciences and Engineering, Cardiff University, UK
[2] Université d'Orléans, Laboratoire PRISME EA 4229, F45072 Orléans, France
Corresponding authors email: (*) mashruks@cardiff.ac.uk

(**) seif-eddine.zitouni@univ-orleans.fr

Abstract

Ammonia, a carbon-free source of hydrogen has recently gained considerable attention as energy solution towards a green future. Previous works have shown that adding $30_{VOL.\%}$ hydrogen with ammonia can eradicate the drawbacks of pure ammonia combustion but no study in the literature has investigated this blend across a wide range of equivalence ratios. The present work investigates $70/30_{VOL.\%}$ NH_3/H_2 blend from $0.55 \leq \Phi \leq 1.4$ for both premixed laminar spherically expanding flames and turbulent swirling flames at atmospheric conditions. A detailed chemistry analysis has been conducted in Ansys CHEMKIN-PRO platform using a chemical reactor network (CRN) model to simulate the swirling turbulent flames. NO and NO_2 emissions have followed similar bell-shaped trends, peaking at around $\Phi = 0.8$, while N_2O emission rises at lean conditions ($\Phi \leq 0.7$). The results indicate that $\Phi = 1.2$ is the optimum equivalence ratio with reduced NO_X emissions and some ammonia slip.

Keywords: ammonia, hydrogen, flame speed, NO_X, chemiluminescence

1. Introduction

Ammonia, a chemical that is globally employed for fertilizing applications, has also demonstrated to be capable to deliver high power outputs for the industry and the power sector when burned directly or partially mixed with various doping agents (ie. hydrogen, methane, coal, methanol, etc.). Ammonia is the second most commercialised chemical. It is globally traded (about 10% global production) and stored within an existing infrastructure that includes over 120 ports worldwide [1]. Its use can also serve for industrial heating processes feedstock and maritime systems, with the latest being the most probably to reach commercial maturity in the short term. Ammonia has been also conceived as a hydrogen carrier, although its cracking would require at least 15% (and up to 33%) of heat supplied, thus accounting to the losses of the available energy in the molecule. Although the energy could come from waste heat as an alternative [2], it is likely that this would serve just to partially crack ammonia, as ammonia blends are showing to be promising solutions for the generation of power and propulsion. Therefore, ammonia-based blends have demonstrated to be reliable as means to reduce carbon, improve storage, and be competitive with fossil fuels, Fig. 1.

However, maritime, transport, heating and power still require advanced technological improvements, with internal combustion engines, furnaces, and gas turbine manufacturers already involved in programs that promise large power outputs by 2024 [3]. Within the technological needs under scrutiny, toxicity, corrosivity and unwanted emissions top the list of areas that scientists and technologist are currently trying to tackle. Emissions, especially NO_X, are extremely complex, being a subject under research that has not been solved over decades. Therefore, considerable efforts are under way to mitigate NO_X in ammonia combustion systems, although there are still many phenomena barely understood around the production of these contaminants.

Type	MGO	LNG	Bio gas	Bio diesel	Methanol	Ammonia	Hydrogen
Carbon	Fossil Fuel		Carbon neutral				
Storage condition	Ambient temperature and pressure	-162°C	-162°C	Ambient temperature and pressure	Ambient temperature and pressure	-34°C or 10bar	-253°C
Relative fuel tank size	1	2.3	2.3	1	2.3	4.1	7.6
Relative CAPEX	1	1.3	1.3	1	1.15	1.2	Very expensive
Fuel cost & availability	Less expensive, high availability		Supply constraints mean this isn't a large scale option	Difficult to forecast due to unstable supply and food security issues	Expensive due to high cost of CO2 capture	Expensive compared to fossil fuel but low priced for carbon neutral	Reasonable fuel production cost. High storage and transport cost

Fig. 1. Comparison between different energy vectors [4].

Nitrogen oxides are formed in most combustion processes that use air as reactant. Mostly, nitric oxide (NO) is formed, with small traces of nitrogen dioxide (NO_2) and nitrous oxide (N_2O). These molecules are precursors of acid rain, photochemical smog and greenhouse effects (i.e. N_2O). Out of the three mechanisms from which NO_X can be formed (i.e. thermal, prompt or fuel-based), fuel-based NOx are the most stringent in ammonia combustion systems.

In 1960, studies by [5] were conducted to understand the oxidation of nitrogenated fuels such as ammonia. Miller and Bowman [6] proposed a mechanism for NO_X formation and removal processes, demonstrating that NO/N_2 formation mainly depended on the path of NH_X radicals. Lindstedt et al. [7] developed a mechanism that recognised important reactions for the formation of NO. Skreiberg et al. [8] established a detailed chemical kinetic model that emphasized the impact of low temperatures on the path $NH_3 \rightarrow NH_2 \rightarrow N_2$, whilst $NH_3 \rightarrow NH_2 \rightarrow NH \rightarrow N$ was raised as main reaction path, and formation of NO, at higher temperatures.

Further studies developed by Konnov et al. [9], Duynslaegher et al. [10], Tian mechanism [11], Mendiara and Glarborg [12], Brackmann et al [13], etc. confirmed the impact of OH, H_2, O, O_2 and H_2O on the production of HNO, one of the main precursors of NO during ammonia combustion. Mathieu and Petersen [14] studied the oxidation of ammonia under high temperatures (1560–2455K) and high pressures (up to 3.0 MPa). A detailed mechanism model was established. Xiao et al. [15] conducted analyses of various kinetic models, leading to further improvements of established models for the study of industrial conditions. Okafor et al. [16] investigated the reaction of various molecules and successfully integrated GRI-Mech 3.0 and Tian's models, delivering good results when using ammonia-methane blends. Further works by Glarborg et al. [17] enabled a more holistic mechanism that encompassed the most important nitrogen reactions when burning NH_3. The model has been assessed and compared to other chemical kinetic mechanisms [18] showing good results.

The work showed that fuel NO formation/reduction is dependent on the O/H radical pool, which varies depending on equivalence ratio and pressure conditions. Further, it was highlighted that there is a competition between NO and nitrogen-based radicals on the pools of chemical existing in these types of flames. Ramos et al. [19] assessed the use of ammonia with methane, experimentally and numerically investigating NO_X and CO profiles. After comparing various mechanisms, it was found that HNO reactions with OH and H radicals play the most crucial role in the formation of NO. Further works performed by Shu et al [20] in auto-ignition kinetics of ammonia at various temperatures and pressures were developed to understand ammonia and NO chemistry. Shrestha et al. [21] and Otomo et al. [22] are also reaction mechanisms that have demonstrated their application in engines and hydrogen doped systems, respectively. However, it has been still evident that models tend to over/underpredict some radicals and emissions, and this has become evident with the case of NO, N_2O or NO_2. Recent work performed by experimentalists trying to find methods for NO reduction in small furnaces [23], fundamental studies of complex stratified injection methodologies that demonstrate ammonia diffusion and O/H reactivity in NO mitigation [24], applied semi-industrial

emissions monitoring and the interaction of NH_X in NO impact [25], and large power facility initiatives whose target is large production with minimum emissions [26], are all examples of the vast work that is currently taking place to reduce NO_X in ammonia combustion systems.

In the case of N_2O, which as previously mentioned is a highly potent greenhouse gas, the existing literature for ammonia combustion systems is scarce. Lee et al. [27] studied hydrogen/ammonia/air flames and found that by increasing ammonia content under lean conditions can substantially increase the production of N_2O. Similarly, Okafor et al. [28] demonstrated in ammonia/methane flames that lean conditions can be detrimental to the production of N_2O, with the heat losses of lean conditions being main culprits of these features. This was further studied via wall-temperature analyses, which shod that the low temperature were main drivers of the high N_2O production. However, more experiments are required to fully understand the behaviour of N_2O in ammonia flames, as the production of the former can considerably mitigate the rationale of a "zero emissions, climate friendly" system. Recent publications [29–31] suggest that N_2O appears not only in the lean regime, but also the very rich regions, thus posing a threat to the use of ammonia combustion under these regimes. However, it must be emphasized that there remain many unknown aspects of the production of this molecule using ammonia fuelling [32].

Clearly, although ammonia offers several advantages, with storage requirements similar to those of other energy vectors, see Fig. 1, there remains several combustion challenges notably the control and reduction of pollutant emissions (NO_X and N_2O). Moreover, ammonia exhibits slow burning velocities, often associated to low burning efficiencies in engines, high ignition energy as well as a narrow flammable range, potentially resulting in poor flame stabilisation and extinction characteristics resulting in local or global extinctions. As such there seems to be a practical necessity to develop and strengthen understanding of fundamental combustion characteristics of multi-fuel blends containing NH_3, ultimately leading to the development of combustors offering greater flame stability and reduced pollutant emissions. The laminar burning velocity, is a fundamental physio-chemical property of a premixed combustible mixture, reflecting both the combustion process and mixture reactivity. As such, the laminar burning velocity is a key parameter helping describe premixed operational instabilities, notably flashback, blow-off or extinction, and a central step in turbulent flame modelling, as well as reaction mechanism validation [33].

Recent experimental studies have investigated the laminar burning velocity of ammonia/air flames, notably Hayakawa et al. [34], at atmospheric and high pressure (0.5 MPa) whilst Kanoshima et al. [35] investigated the influence of temperature (400 – 500 K). Results from these works highlight that the laminar burning velocity of ammonia/air peaks at an equivalence ratio (Φ) of ~1.05 – 1.10, with an increase in pressure and temperature resulting in a decrease and increase in laminar burning velocity, respectively. Supplementary fuels such as Hydrogen have been shown to improve the combustion performances of ammonia. Lhuillier et al. [36] produced an extensive dataset of laminar burning velocities for ammonia/hydrogen mixtures at various initial conditions (298-473K, $\Phi = 0.8 – 1.4$, $H_2 = 60\%$ vol. max), with further work on ammonia/hydrogen also available in [37]. For up to 20 to 30% Hydrogen addition, both aforementioned studies highlight a linear correlation between added molar hydrogen fraction and flame speed of hydrogen/ammonia blends, prior to an exponential increase in flame speed upon further hydrogen addition.

A fuel blend with an ammonia/hydrogen of $70/30\%_{VOL}$ was specified for this work. Alternative blends have previously been appraised [38], with the selected blend demonstrating to exhibit the most stable performance between a propensity to flashback manifest with greater Hydrogen fraction (> 40%) as well as blow-off stability under richer conditions. Furthermore, this blend has previously been demonstrated to behave in an analogous manner to that of a premixed methane flame [39,40]. Furthermore, under lean conditions, the selected blend exhibits flame speeds comparable to those of methane/air flames.

The aim of the work presented in this study attempts to progress on the practicalities of using $70/30\%_{VOL}$ ammonia/hydrogen blend at a wide range of equivalence ratios by investigating both swirling turbulent flames and laminar flames, whilst addressing the complex nature of NO_X formation, with special emphasis on the production of NO, N_2O and NO_2. Employing advanced emission measurements, non-intrusive optical techniques and a constant volume vessel to measure laminar burning velocities, a set of experiments has been compiled to deliver reliable data useful for model and reaction validations. As previously raised, the applied aspect of this work goes beyond the area of just combustion, and can be employed in the validation of numerical models of novel ammonia-based power designs.

2. Experimental Facility

2.1. Constant Volume Combustion Vessel

Laminar flame speed measurements were performed using a constant-volume spherical vessel as shown in Fig. 2. Details of the rig and post-processing technique can be found in [41], updated for NH_3 specifications in [36] and thus only a brief summary is presented here. The spherical vessel has a nominal internal volume of 4.2 L (ID 200mm), with four orthogonal 70 mm quartz viewing windows with PID temperature control. High-speed Schlieren imaging of flame propagation was achieved using a CMOS high speed camera (PHANTOM V1210 (±0.05%)) set to a suitable fast frame capture rate and facilitating a spatial resolution of ~0.1 mm per pixel. Flame propagation rates were calculated by edge-detection algorithms written into a bespoke MATLAB script. Reactants were introduced into the chamber using batched thermal mass flow controllers (Brooks 5850S (±1%)). Mass fractions were calculated as a function of initial pressure (P), fuel-air equivalence ratio (Φ), and temperature (T), with mixture concentrations confirmed by partial pressure. Internal fans were used to pre-mix the reactants, and capacitor-discharge ignition was achieved via fine electrodes mounted to 45° to the measurement plane. Experiments were triggered by a simultaneous TTL signal to the ignition system and data acquisition systems after quiescence had been attained. High-purity fuel components of H_2 (>99.95%) and NH_3 (99.95%) and dry-zero grade compressed air were used to perform the experiments. Measurements were performed at initial conditions of 298 K (± 3K) and 0.1MPa (± $1x10^{-3}$Mpa).

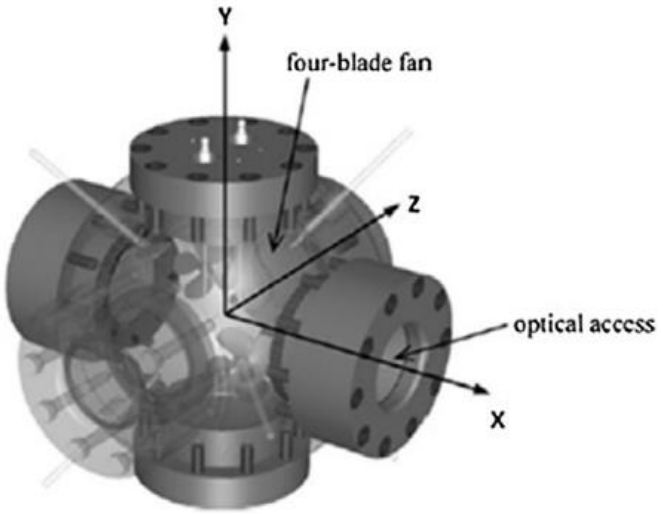

Fig. 2. Schematic of Constant Volume Combustion Vessel

To investigate the influence of H_2 on NH_3 flame propagation, spherically expanding flame experiments were conducted for a set mol ratio of H_2 (30%, vol.), evaluated across a wide range of equivalence ratio (0.6 – 1.4), to provide a comparison of the change in flame speed from lean to rich conditions. Schlieren measurements were undertaken to evaluate the laminar burning velocity relative to the burned side, experimentally determined employing the same procedure as in previous studies [36,42]. The quasi-steady non-linear association between the stretched flame speed and stretch was employed [43] – rearranged with the error used for least square regression – to obtain an extrapolated unstretched flame speed. The adiabatic expansion at constant pressure (defined as the ratio of the burnt (ρ_b) to unburnt (ρ_u) densities, $\sigma = \rho_b / \rho_u$) was accounted in order to obtain representative values of laminar flame speed, with average results plotted in subsequent figures illustrating laminar burning velocities. A minimum of 5 repeats were conducted per experimental condition.

2.2. Swirl Burner

The employed axial swirl burner with a swirl number, S_g = 1.05, is presented as a cross-sectional schematic in Fig. 3, with a constant thermal power of 8kW at atmospheric conditions (288±5 K and 0.11±0.005 MPa). An ammonia/hydrogen blend consisting of 70/30% (vol) was selected on the basis of previous experiments [44] that demonstrated the high stability, low emissions and low hydrogen requirements (ie. from ammonia cracking) of such a blend. Further, such a blend has never been fully investigated over a wide range of equivalence ratios under laminar and turbulent propagation conditions.

Ammonia and air were introduced at the bottom of the mixing chamber, while hydrogen was injected through 6 radially equispaced holes (1.5 mm diameter) at the central lance, located 40 mm below the burner exit, angled at 45°, directly releasing hydrogen into the swirler to ensure premixing with ammonia and air prior to ignition. Bronkhorst mass flow controllers (±0.5% uncertainty within a range of 15-95% mass flow) were used to control the flow rates of fuel and air, as per the conditions stated in Table 1. Chemiluminescence measurements were taken perpendicular to the reactant flow direction through the quartz tube, specified to give enhance UV transmission. Greater detail of the facility can be found in other publications [29,31].

Table 1. Summary of experimental matrix.

Parameter	Value	Parameter	Value
Ammonia mol fraction, X_{NH3}	0.70	Inlet Temperature	288±5 K
Thermal Power	8 kW	Inlet Pressure	0.11±0.005 MPa
Equivalence Ratio (Φ)	0.55 – 1.4 (steps of 0.05)	Outlet Pressure	0.10±0.005 MPa

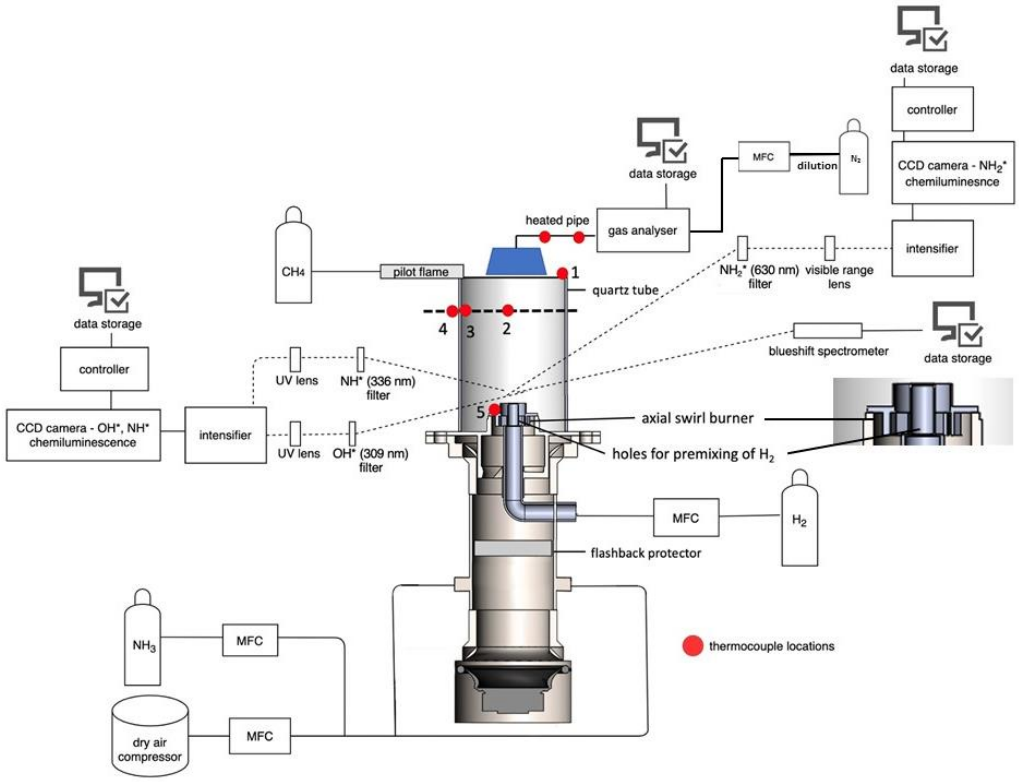

Fig. 3. Cross-sectional schematic of the swirl burner with measuring techniques and data acquisition systems.

2.3. Chemiluminescence

Chemiluminescence measurements were obtained at each experimental condition for the turbulent ammonia/hydrogen/air swirling flames, targeting electronically excited intermediate chemical radicals within the flames. The species investigated were OH* near 309 nm [45], NH* near 336 nm [45–48] and the α band of NH_2 near 630 nm [45,49], captured using combinations of a pair of Lavision Image Intense CCD cameras, dedicated IRO image intensifiers, UV and visible lenses, and narrow bandpass filters selected specifically for each species. The units were triggered simultaneously at a frequency of 10 Hz with constant gain. The image resolution is 6.2 pixels/mm for the UV lens and 4.8 pixels/mm for the visible lens, resulting in a field of view of 70 mm (axial, y) by 100 mm (radial, x) relative to the edge and centreline of the burner exit nozzle, respectively. LaVision Davis v10 was used to gather 500 frames for each data point, which were then background subtracted, temporally averaged and post-processed using a bespoke MatLab script [50] designed to conduct Abel Deconvolution with the assumption of flame symmetry, following a 3 x 3 pixel median filter, as per [51–53]. Colourmaps of the chemiluminescence images have been normalised to the maximum intensity of each image to display the changes in species distributions for each flame.

A UV/visible-capable optical fiber head (Stellernet Inc DLENS with F600 fiber optic cable) was installed 3 cm above the burner's exit and 10 cm away from its central axis. The other end of the optical fiber was connected to a UV/visible-capable spectrometer (Stellernet Inc BLUE-Wave) featuring a 100-mm focal length and a 25-µm wide entry slit. The spectrometer was equipped with a 600-grooves/mm grating and a Si-CCD detector (Sony ILX511b) featuring 2048 effective pixels of size 14×200 µm^2, yielding a spectral resolution of 0.5 nm. The detector's exposure time was set to 1 sec and 20 scans were averaged to improve the signal-to-noise ratio (SNR). The Y-axis of the spectrometer was calibrated using a standard light source (SL1 Tungsten Halogen).

2.4. Emissions

Exhaust emissions (NO, N_2O, NO_2, NH_3, O_2 and H_2O) were measured using a bespoke quantum cascade laser analyzer (Emerson CT5100) operating at 463 K with a sampling frequency of 1 Hz (±1%, 0.999 linearity). Dilution methodology was introduced by adding N_2 in the sample using high precision Bronkhorst EL-FLOW Prestige MFC. The N_2 then get heated up to 160°C by the system prior to mixing with the exhaust samples. The flowmeter of the analyser is calibrated by the manufacturer and this is enough for its usual purpose. The flow rate of the exhaust process sample in the system during dilution methodology is then calculated by Eq. (1).

$$\text{Exhaust sample flow rate } (F_S) = \text{Total intake flow rate } (F_t) - \text{Dilution } (N_2) \text{ flow rate } (F_d) \quad (1)$$

An isokinetic funnel with an intake diameter of 30 mm was fixed at 50 mm above the quartz confinement's exit to capture homogeneous samples from the exhaust for selected operating conditions. All the emissions data reported here were recorded and averaged over a period of 120 s.

2.5. Temperature

Temperature profiles were obtained at five locations (red dots, Fig. 3) via K and R type thermocouples feeding a data logger with a frequency of 1 Hz. Thermocouple data were taken for 120 s for each point and averaged. The thermocouples were calibrated showing an average error of 3% of reading. The acquired temperature data were corrected as per [54] to account for the convective and radiative heat transfer of the thermocouples with their surroundings, as well as conductive heat transfer between the thermocouple bead and the connecting thermocouple wires.

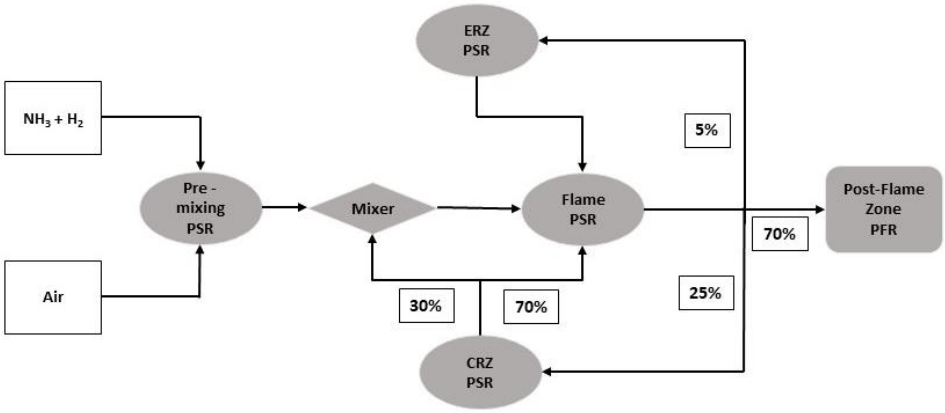

Fig. 4. Chemical reactor network (CRN) model structure.

3. Chemical Reactor Network (CRN) Modelling

A chemical reactor network (CRN) model was developed to simulate the chemistry of the experimental swirling ammonia/hydrogen/air flames [25,55,56]. Inlets were used to provide fuel and air flows, with four perfectly stirred reactors (PSR) to model the pre-mixing, flame, central recirculation zone (CRZ) and external recirculation zone (ERZ). The recirculation strength was determined by previous experimental campaigns that employed comparable industrial

scale swirl burners [57,58]. The outlet from the flame zone fed a plug flow reactor (PFR) to simulate reactions in the post-flame zone. The model structure is outlined in Fig. 4 and was established with representative combustor geometry. The residence times were calculated from empirical flow conditions and heat loss was estimated from the corrected thermocouple measurements. It should be emphasized that moderate uncertainty is associated with CRN modelling, and the system developed was primarily used to identify the significant reactions, rather than detailed prediction. In order to employ the model efficiently, various reaction mechanisms including Stagni et al. [59], Gotama et al. [60] and Glarborg et al. [61] are appraised with respect to the laminar burning velocity, presented in the following section. The model employed the reaction mechanism developed by Stagni et al. [59] for NH_3-H_2-air mixtures, with 31 chemical species and 203 reactions; appraised using the laminar burning velocity measurements as well as having shown good performance for NH_3/H_2/air blends in recent studies [37,58,62].

4. Results and Discussions

4.1. Laminar Flame Speed Measurements

Fig. 5 presents the measured laminar burning velocities for the $70/30_{VOL.\%}$ ammonia/hydrogen blend alongside values attained numerically employing the Stagni et al. [59], Gotama et al. [60] and Glarborg et al. [61] reaction mechanisms. For comparison purposes, the measured laminar burning velocity, of pure ammonia and methane are illustrated in Fig. 5.

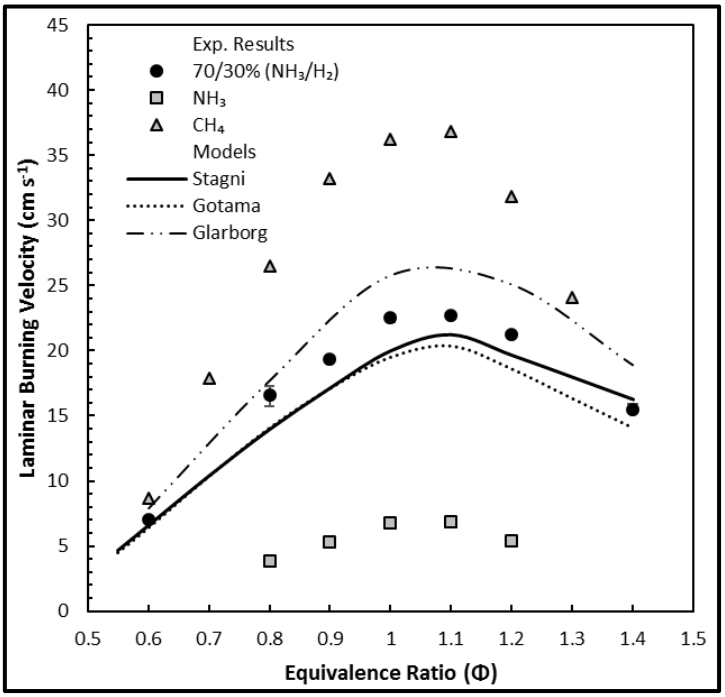

Fig. 5. Laminar burning velocity for $70/30\%_{VOL}$ Ammonia/hydrogen blend as a function of equivalence ratio. Model results from Stagni et al. [59], Gotama et al. [60], Glarborg et al., [61] – T_u = 298K, P_u= 1 bar

As can be seen from Fig. 5, the addition of 30% hydrogen to ammonia-based flames results in significant relative increases in flame speed, with this effect most pronounced at leanest and richest conditions (at Φ 0.80 and 1.20 relative increase in flame speed ~ 300%, evaluated on a percentage basis). With respect to reaction mechanism appraisal, no reaction mechanism satisfactorily captures the measured flame speeds across the entire air fuel ratios evaluated. Best agreement is displayed with the Stagni reaction mechanism with present experimental results, although it is noted that modelled results underestimate the laminar burning velocities of the selected blend.

The CHEMKIN-Pro-package employing the PREMIX module, to simulate a 1-D adiabatic planar flame, was used to provide a better understanding of the reactivity trends displayed in Fig. 6. A simulation domain of 10 cm was considered, with a total of 2000 grid points used, including multi-component diffusion and an assumed air composition of 79% N_2 – 21% O_2. The Stagni reaction mechanism was utilised to generate volumetric heat release rates (Q') and concentration of mole fractions of active radicals (H, OH, NH and NH_2). Relative changes in measured flame speed and numerically attained Q', selected radical mole fractions, normalised to that of pure ammonia for Φ 0.8 - 1.2 are presented in Fig. 6.

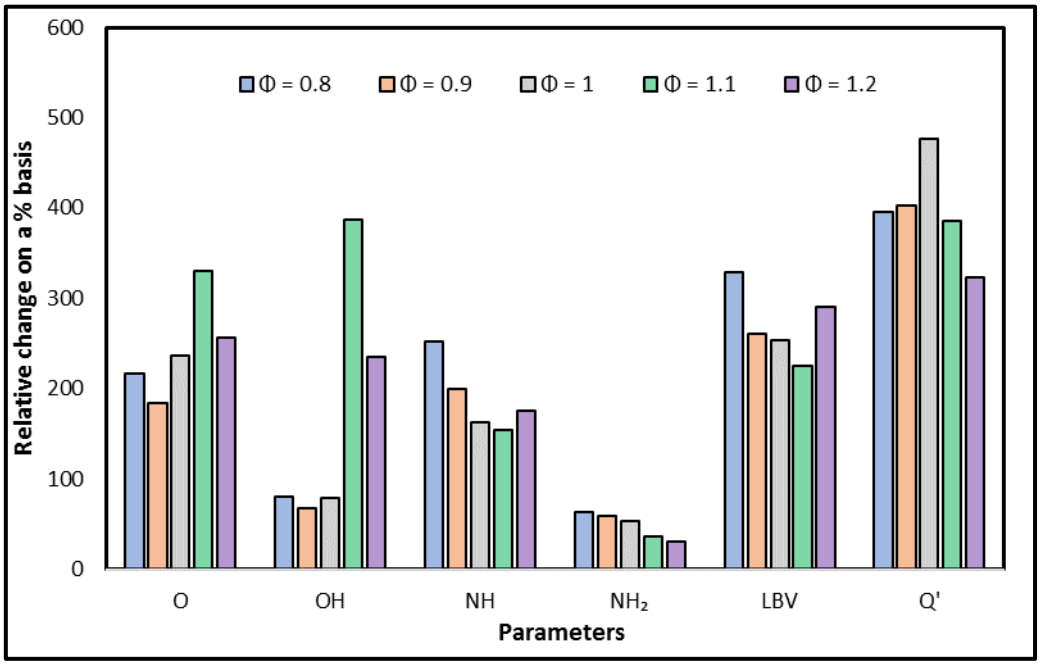

Fig. 6. Relative changes in measured laminar burning velocity and modelled Q', H, OH, NH and NH_2 mole fraction concentrations, normalised to that of pure Ammonia for NH_3/H_2 (70/30%$_{VOL}$) blend at Φ 0.8 – 1.2.

As can be seen from Fig. 6, addition of 30%$_{VOL.}$ hydrogen to ammonia-based fuels results in an increased reactivity, with relative changes in flame speed (LBV in Fig. 6) most important at richest and leanest conditions, with this same trend displayed by the production of NH radical. Interestingly, relative changes in flame speed and burning intensity (Q') follow opposite trends, different to what is traditionally observed in methane/hydrogen combustion [42]. Unsurprisingly, production of O radicals appear to be highly correlated with heat release whilst relative changes of NH_2 production decreases with increasing equivalence ratio, due to the decreasing presence of O_2.

4.2. Swirling Flames

Fig. 7 illustrates distributions of Abel-Deconvoluted OH*, NH* and NH_2* electronically excited radicals for 70/30$_{VOL.\%}$ NH_3/H_2 flames at $0.6 \leq \Phi \leq 1.4$. Note that the origin corresponds to the burner centreline. The flames are stabilized around a conical shear layer of zero axial velocity, with CRZ and ERZ, typical for a swirling premixed configuration [63–65]. Radical distributions are centred near the origin for Φ = 0.6 and with increasing equivalence ratio, areas of radical distributions expand and drives near the burner wall at the rich conditions with eventual lifting is observed at $\Phi \geq 1.2$ due to the balance between flame speed and inlet gas speed. Fig. 8 shows chemiluminescence spectrum of 70/30$_{VOL.\%}$ NH_3/H_2 blend with changing Φ. Measured OH* and NH* intensities were found to be significantly lower than NH_2* across all conditions considered here. NH_2* intensities increase with equivalence ratio until Φ = 1.2 and then decreases due to severe loss in oxygen availability, resulting in ammonia slips. Radicals in UV range, OH* and NH* peak at Φ = 0.8 and then decreases with increasing equivalence ratio. These observed trends will be analysed further in the latter parts of discussions. Previous work [66] has assumed direct proportionality between ground state and electronically excited species in ammonia disassociation process despite the complicated relationships between them due to various effects such as quenching and radiation losses. However, proportionality is not assumed in the current work, only a positive correlation between emitting and ground state species is applied with more emitting species indicating increase in ground state population [48,53,67,68].

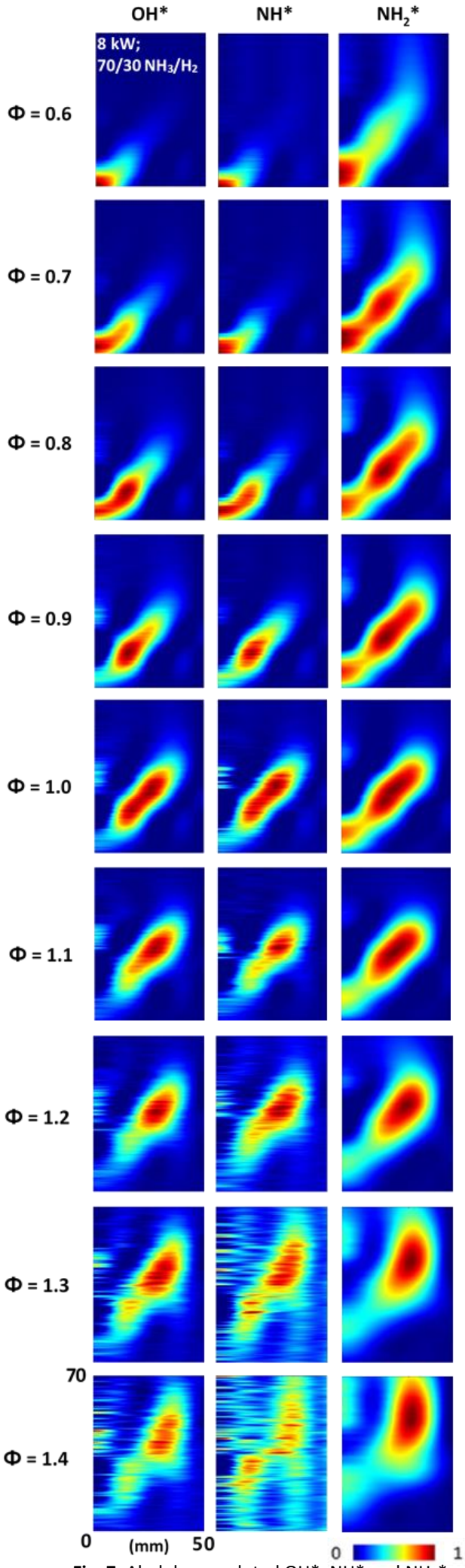

Fig. 7. Abel deconvoluted OH*, NH* and NH_2* chemiluminescence for 70/30$_{VOL.\%}$ NH_3/H_2 flames with increasing Φ. Colormap normalized to image dataset maximum.

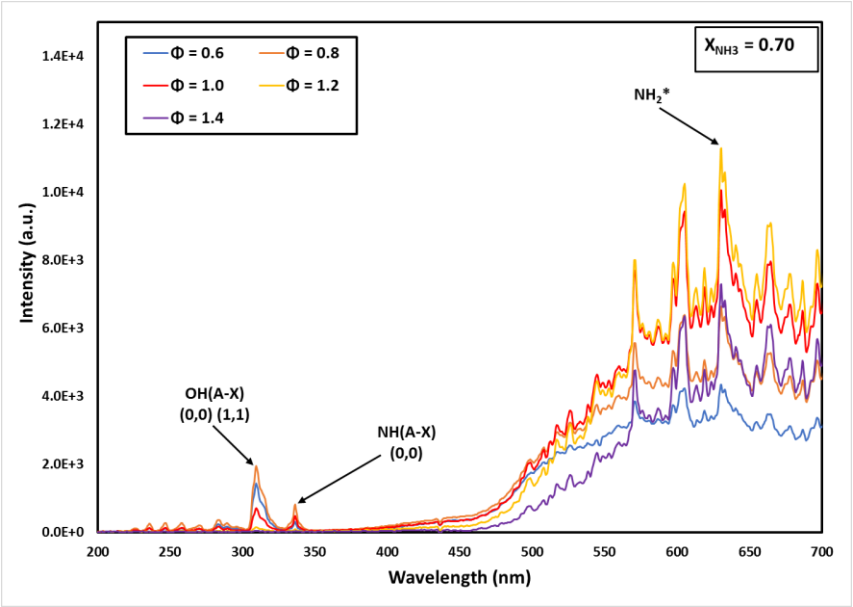

Fig. 8. Chemiluminescence spectrum of 70/30$_{VOL.\%}$ NH_3/H_2 flames with changing Φ.

4.2.1. Emissions Performance

Fig. 9 displays measured wet NO (empty) and NH_3 (shaded) emissions, as well as modelled predictions (lines) including H_2 productions against Φ for premixed $70/30_{VOL.\%}$ NH_3/H_2 flames. The overall trends of modelled and sampled emissions display favourable agreements with some exceptions. NO productions increase with increasing equivalence ratios until Φ = 0.9 and then drops significantly as the flames transit towards rich conditions. Ammonia slips were observed at rich conditions due to the reductions in available oxygen. Modelled ammonia emissions were unable to capture the measured data at Φ = 0.55 and 1.05 ≤ Φ ≤ 1.15. This can be attributed to the dynamic regime shift at low-intermediate temperature regions (900 – 1350 K) [69], which corresponds to very lean and rich conditions, indicating the necessities in further development of more accurate reaction mechanisms. The model also predicted sharp release of H_2 at rich conditions, a vital requirement to enable flameless combustion at the lean stage of two-stage burner configuration to ensure complete combustion of ammonia [55].

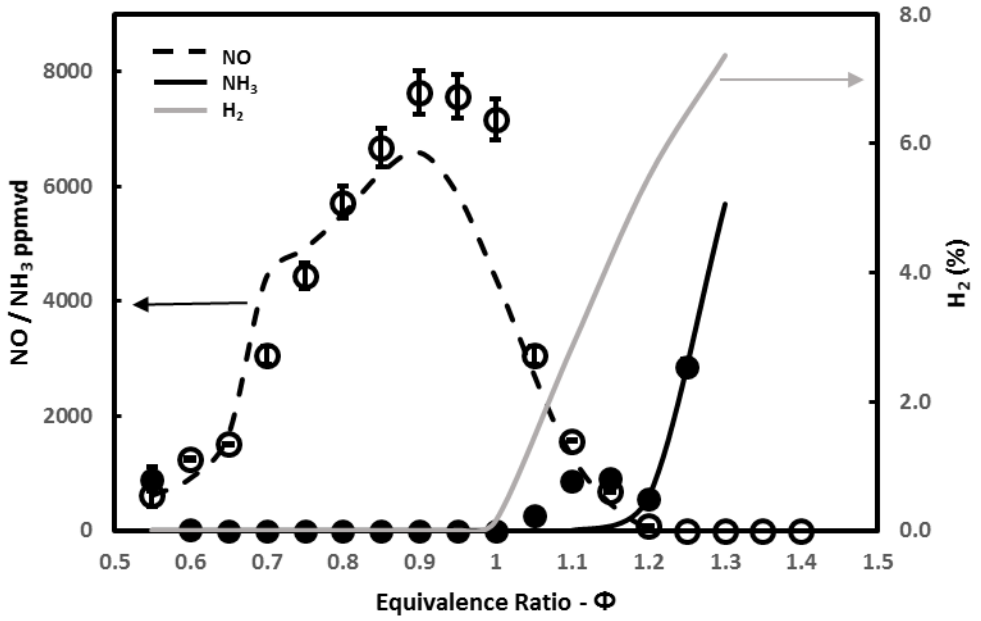

Fig. 9. Measured and modelled NO (empty) and NH_3 (shaded) emissions for $70/30_{VOL.\%}$ NH_3/H_2 flames with changing Φ, alongside simulated H_2 concentrations.

Calculated absolute ROPs of [NH_3] and [NO] at the flame zone are shown in Figs. 10 and 11, respectively. The main oxidation path of NH_3 is through the reaction with OH radicals to produce NH_2 radicals, which has been shown to play the role of heat release marker for NH_3/H_2 [57] and CH_4/NH_3 [70] flames. Reactivity of this reaction decreases as Φ increases from 0.8 to 1.2 due to the reduction in OH availability, as evident by Figs. 7 and 8. The other sources of conversion of NH_3 to NH_2 are through the reactions with O and H radicals. These radicals are related to each other through the reaction $O_2 + H \leftrightarrow O + OH$ to produce O and OH radicals while atomic H is mainly produced when H_2 reacts with OH radicals [55]. These radicals also play vital roles to convert NH_2 radicals to NH radicals. NH_2 and NH radicals convert to HNO by reacting with O and OH radicals, respectively. Measured NH* and OH* radicals intensity peaks at Φ = 0.8, Fig. 4, indicating most HNO production at this condition. HNO is the main source of fuel NO production in ammonia/hydrogen flames through the reactions with atomic H and excess molecular O_2 (at lean conditions). Another source of NO formation is through the Zel'dovich mechanism. However, this source of NO production diminishes at rich conditions due to reduced availability of OH radicals [71–73] and combination with HNO [40,53]. NO reacts with NH and atomic N to produce N_2O and N_2, respectively. Additionally, NO consumption enhances through the chain branching reaction $NH_2 + NO \leftrightarrow NNH + OH$ and the terminating reaction $NH_2 + NO \leftrightarrow N_2 + H_2O$ [57,74].

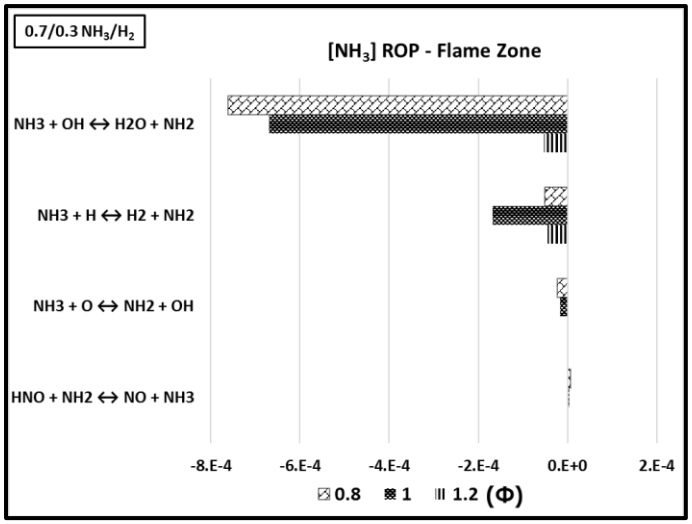

Fig. 10. Absolute ROPs of [NH_3] for 70/30$_{VOL.\%}$ NH_3/H_2 flames with changing Φ. [Unit – mole/cm^3-sec].

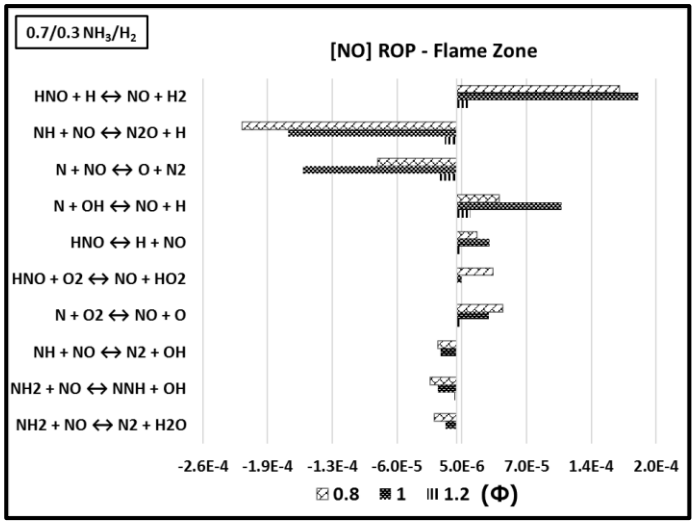

Fig. 11. Absolute ROPs of [NO] for 70/30$_{VOL.\%}$ NH_3/H_2 flames with changing Φ. [Unit – mole/cm^3-sec].

Changes in measured NO_2 (empty) and N_2O (shaded) emissions with Φ are shown in Fig. 12. The markers show the averaged wet experimental data, with results from the CRN model represented by lines. The model also allows for the simulation of exhaust N_2 concentrations, which were not measured and shown to gradually decrease with increasing Φ. The available N_2 from the air mostly remains unreactive, while further N_2 is produced through flame reactivity. Reactivity of these reactions decreases with increasing Φ, which in collaboration with reduced N_2 availability from air deficiency reflect into reduced N_2 concentrations as the flame goes richer. Sampled NO_2 reading peaks at around Φ = 0.8, similar to NO reading, with significant drops in production at either side of the peak. N_2O emissions are evident for Φ ≤ 0.7. Even though CRN predictions for N_2O are very closed to sample data, NO_2 predictions are out by a factor of ~12. These discrepancies between modelled and sampled data, as well as the observed emissions trends are analysed in the following section.

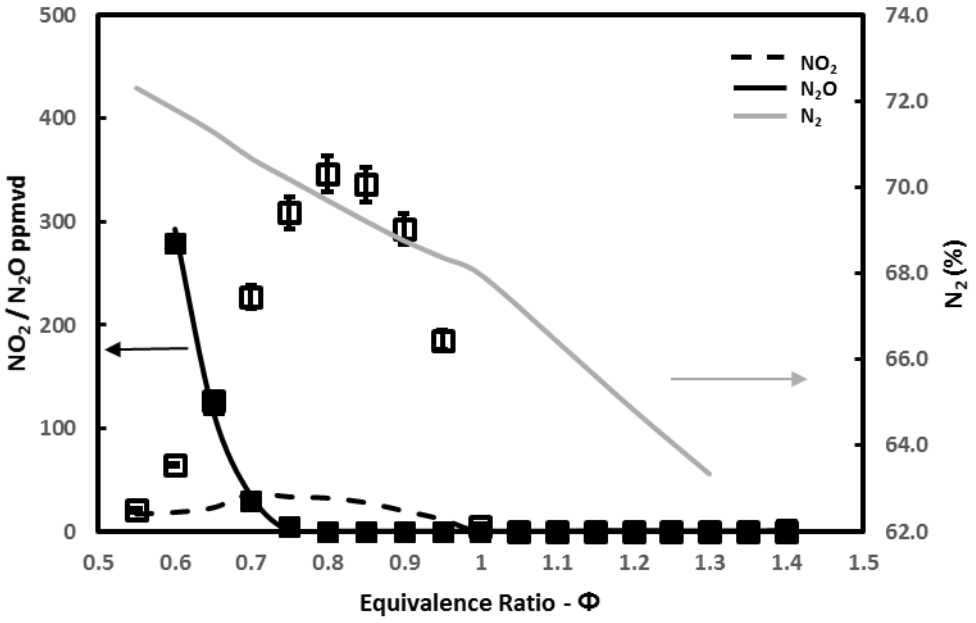

Fig. 12. Measured and modelled NO_2 (empty) and N_2O (shaded) emissions for 70/30$_{VOL.\%}$ NH_3/H_2 flames with changing Φ, alongside simulated N_2 concentrations.

Figs. 13 and 14 illustrate the calculated ROP at the flame zone with changing Φ for [NO_2] and [N_2O], respectively. NO_2 is mainly produced in the flames when NO reacts with hydroperoxyl or through the third body reaction NO + O + M ↔ NO_2 + M, whereas NO_2 converts to NO by reacting with O and H radicals mainly at the lean conditions due to the presence of excess oxygen. Recent work [30] has shown that the third body reaction is the most prominent route for NO_2 production at the post-flame zone. The discrepancy between the model predictions and sampled NO_2 emissions can be attributed to the dependency on the third body reaction to produce NO_2 as ammonia has higher third body efficiency compared to other fuels [75] which has not been considered in the existing ammonia oxidation reaction mechanisms. Considerable amount of NO converts to N_2O at the flame zone through the reaction NH + NO ↔ N_2O + H. This reaction is dependent on the availability of NH radicals which reduces with reduced availability of air as evidenced by Figs. 3 and 4. However, most of this N_2O produced at the flame zone converts to molecular N_2 by reacting with H radicals and through another third body reaction N_2O + M ↔ N_2 + O + M. Earlier studies [56,76] have shown that this third body reaction has very high activation energy requirements and its reaction rate suffers at low temperature conditions which is in line with the high N_2O concentrations measured at Φ < 0.7 as shown in Fig. 8, due to decreased flame temperature.

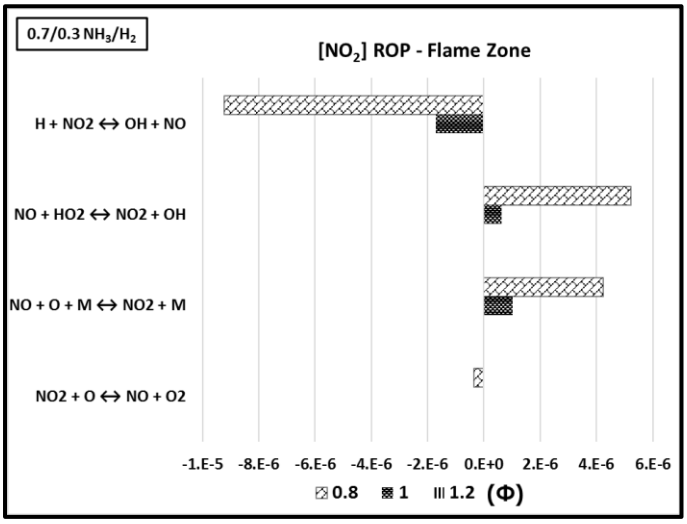

Fig. 13. Absolute ROPs of [NO_2] for 70/30$_{VOL.\%}$ NH_3/H_2 flames with changing Φ. [Unit – mole/cm^3-sec].

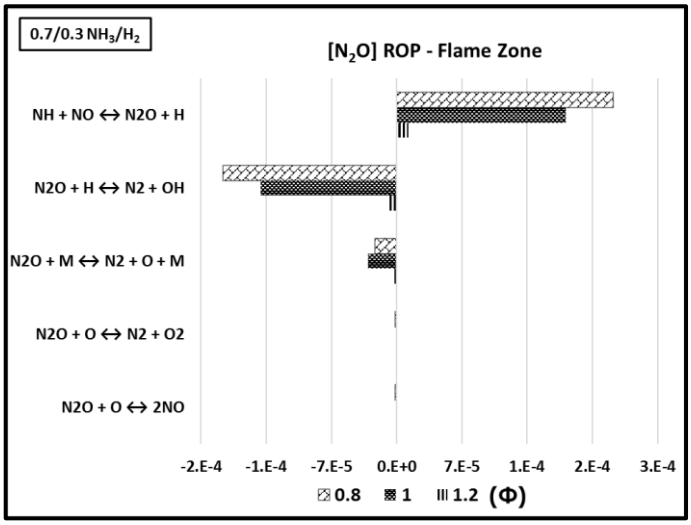

Fig. 14. Absolute ROPs of [N_2O] for 70/30$_{VOL.\%}$ NH_3/H_2 flames with changing Φ. [Unit – mole/cm^3-sec].

5. Conclusions

This study investigated premixed 70/30$_{VOL.\%}$ NH_3/H_2 blend under atmospheric condition at a wide range of equivalence ratios (0.55 – 1.4) for both spherically expanded laminar and swirling turbulent flames. Laminar burning velocities of the blend under investigation were compared with pure ammonia and methane flames. Results from three ammonia-based reaction mechanisms were compared against the experimental data for validation purposes with Stagni's mechanism performing closest to the experimental data. Swirling turbulent flames were investigated with a combination of spatially resolved OH*, NH* and NH_2* chemiluminescence, spectrometry analysis and sampled exhaust emissions data. The experimental conditions of the swirling flames were evaluated numerically in Ansys Chemkin-Pro environment by employing a CRN model and utilizing Stagni's mechanism to identify the significant reactions responsible for NO_X emissions. The main conclusions of this study are summarised as follows.

1. Addition of 30%$_{VOL.}$ H_2 to NH_3 significantly enhanced the flame speed compared to the pure ammonia flames with pronounced improvements at the leanest and richest conditions. Numerical analysis of a 1-D adiabatic planar flame identified increased reactivity with the addition of hydrogen, in terms of radical productions and volumetric heat release rates. Relative percentage changes in O and OH radical peaked at Φ = 1.1, coinciding with the measured peak flame speed while NH radical closely followed the trend of laminar burning velocity and NH_2 production decreases with increasing Φ.
2. Sampled exhaust NO readings peaked at Φ = 0.9, dropping more significantly at the rich side than the lean side while NH_3 emissions were visible at the rich side due to reduction in oxygen availability. HNO was

identified as the main species responsible for fuel NO production while considerable amount of thermal NO was produced through Zel'dovich pathway near stoichiometry due to high flame temperature. Main NO reduction pathways were identified as the reactions with NH radicals and atomic nitrogen, as well as through the ammonia deNOxing routes.

3. Exhaust NO_2 emissions increased with increasing equivalence ratio until Φ = 0.8 and then dropped considerably with no readings beyond stoichiometry. NO found to be responsible to produce NO_2 in flames by reacting with hydroperoxyl and through the third body reaction NO + O + M $\leftrightarrow$ NO_2 + M. Most of the produced NO_2 converted back to NO by reacting with H radicals. CRN model predictions of NO_2 were significantly lower than the sampled NO_2. This discrepancy was attributed to the unaccounted higher third body efficiency of ammonia-based fuels.
4. Sampled N_2O emissions were prominent at $\Phi \leq 0.7$. The reaction between NH radicals and NO was identified as the main source of N_2O production in the flame zone. However, most of this N_2O converted to N_2 by reacting with H radicals and via the third body reaction N_2O + M $\leftrightarrow$ N_2 + O + M. This third body reaction has high activation energy requirements and has been identified as the reason behind the high N_2O emissions at lean conditions ($\Phi \leq 0.7$) with comparatively lower flame temperature.
5. The results reinforced Φ = 1.2 as the point of interest for this blend with minimum NO_X emissions with some ammonia slip which will be oxidised in a two-stage combustion scenario. Simulated concentrations of H_2 and N_2 at the exhaust were also reported with changing equivalence ratios. H_2 concentrations increased sharply beyond stoichiometry and identified as a vital element for flameless combustion in a two-stage combustion system. Gradual decrease of nitrogen concentrations was reported with increasing equivalence ratio due to air deficiency.

As previously underlined, ammonia combustion is gaining considerable attention and thus there seems to be a practical necessity in developing and strengthening understanding of fundamental as well as practical combustion characteristics of multi-fuel blends containing NH_3. The applied aspect of this study and its conclusion attempts to go beyond the area of just combustion, with results provided useful with respect to numerical model validation of novel ammonia-based power designs, ultimately leading to the development of combustors offering greater flame stability and reduced pollutant emissions.

Acknowledgements

This work was supported by the European Union's Horizon 2020 research and innovation programme under grant agreement No 884157 and the SAFE-AGT pilot (no. EP/T009314/1) with funding from the Engineering and Physical Sciences Research Council (EPSRC). The laminar flame speed experiments were undertaken at the University of Orleans PRISME lab. The turbulent flame research was undertaken at Cardiff University's Thermofluids Lab (W/0.07) with invaluable technical support from Mr. Malcolm Seaborne. Information on the data underpinning the results presented here, including how to access them, can be found in the Cardiff University data catalogue at http://doi.org/10.17035/d.2022.0218686600.

References

[1] IRENA, Global Hydrogen Trade to meet the 1.5oC Climate Goal, 2022.

[2] S. Sittichompoo, H. Nozari, J.M. Herreros, N. Serhan, J.A.M. da Silva, A.P.E. York, P. Millington, A. Tsolakis, Exhaust energy recovery via catalytic ammonia decomposition to hydrogen for low carbon clean vehicles, Fuel. (2021). https://doi.org/10.1016/j.fuel.2020.119111.

[3] A. Valera-Medina, F. Amer-Hatem, A.K. Azad, I.C. Dedoussi, M. de Joannon, R.X. Fernandes, P. Glarborg, H. Hashemi, X. He, S. Mashruk, J. McGowan, C. Mounaim-Rouselle, A. Ortiz-Prado, A. Ortiz-Valera, I. Rossetti, B. Shu, M. Yehia, H. Xiao, M. Costa, Review on Ammonia as a Potential Fuel: From Synthesis to Economics, Energy & Fuels. 35 (2021) 6964–7029. https://doi.org/10.1021/acs.energyfuels.0c03685.

[4] The North West Hydrogen Alliance, The role of ammonia in the North West hydrogen economy, 2022.

[5] D.I. Maclean, H.Gg. Wagner, The structure of the reaction zones of ammonia-oxygen and hydrazine-decomposition flames, Symposium (International) on Combustion. 11 (1967) 871–878. https://doi.org/10.1016/S0082-0784(67)80213-3.

[6] J.A. Miller, C.T. Bowman, Mechanism and Modeling of Nitrogen Chemistry in Combustion, Prog Energy Combust Sci. 15 (1989) 287–338. https://doi.org/10.1016/0010-2180(91)90047-F.

[7] R.P. Lindstedt, F.C. Lockwood, M.A. Selim, Detailed Kinetic Modelling of Chemistry and Temperature Effects on Ammonia Oxidation, Combustion Science and Technology. 99 (1994) 253–276. https://doi.org/10.1080/00102209408935436.

[8] Ø. Skreiberg, P. Kilpinen, P. Glarborg, Ammonia chemistry below 1400 K under fuel-rich conditions in a flow reactor, Combust Flame. 136 (2004) 501–518. https://doi.org/10.1016/j.combustflame.2003.12.008.

[9] A.A. Konnov, I. V Dyakov, Measurement of propagation speeds in adiabatic flat and cellular premixed flames of C 2 H 6+ O 2+ CO 2, Combust Flame. 136 (2004) 371–376.

[10] C. Duynslaegher, H. Jeanmart, J. Vandooren, Ammonia combustion at elevated pressure and temperature conditions, Fuel. 89 (2010) 3540–3545. https://doi.org/10.1016/j.fuel.2010.06.008.

[11] Z. Tian, Y. Li, L. Zhang, P. Glarborg, F. Qi, An experimental and kinetic modeling study of premixed NH3/CH4/O2/Ar flames at low pressure, Combust Flame. 156 (2009) 1413–1426. https://doi.org/10.1016/j.combustflame.2009.03.005.

[12] T. Mendiara, P. Glarborg, Reburn chemistry in oxy-fuel combustion of methane, Energy and Fuels. 23 (2009) 3565–3572. https://doi.org/10.1021/ef9001956.

[13] C. Brackmann, V.A. Alekseev, B. Zhou, E. Nordström, P.E. Bengtsson, Z. Li, M. Aldén, A.A. Konnov, Structure of premixed ammonia + air flames at atmospheric pressure: Laser diagnostics and kinetic modeling, Combust Flame. (2016). https://doi.org/10.1016/j.combustflame.2015.10.012.

[14] O. Mathieu, E.L. Petersen, Experimental and modeling study on the high-temperature oxidation of Ammonia and related NOx chemistry, Combust Flame. 162 (2015) 554–570. https://doi.org/10.1016/j.combustflame.2014.08.022.

[15] H. Xiao, A. Valera-Medina, Chemical Kinetic Mechanism Study on Premixed Combustion of Ammonia/Hydrogen Fuels for Gas Turbine Use, J Eng Gas Turbine Power. 139 (2017). https://doi.org/10.1115/1.4035911.

[16] E.C. Okafor, Y. Naito, S. Colson, A. Ichikawa, T. Kudo, A. Hayakawa, H. Kobayashi, Experimental and numerical study of the laminar burning velocity of CH4–NH3–air premixed flames, Combust Flame. 187 (2018) 185–198. https://doi.org/10.1016/j.combustflame.2017.09.002.

[17] P. Glarborg, J.A. Miller, B. Ruscic, S.J. Klippenstein, Modeling nitrogen chemistry in combustion, Prog Energy Combust Sci. 67 (2018) 31–68. https://doi.org/10.1016/j.pecs.2018.01.002.

[18] B. Shu, X. He, C.F. Ramos, R.X. Fernandes, M. Costa, Experimental and modeling study on the auto-ignition properties of ammonia/methane mixtures at elevated pressures, Proceedings of the Combustion Institute. (2020). https://doi.org/10.1016/j.proci.2020.06.291.

[19] C.F. Ramos, R.C. Rocha, P.M. Oliviera, M. Costa, X.S. Bai, Experimental and numerical investigation on NO, CO and NH3 emissions from NH3/CH4/air premixed flames, Fuel. Under Pres (2019).

[20] B. Shu, S.K. Vallabhuni, X. He, G. Issayev, K. Moshammer, A. Farooq, R.X. Fernandes, A shock tube and modeling study on the autoignition properties of ammonia at intermediate temperatures, Proceedings of the Combustion Institute. (2019). https://doi.org/10.1016/j.proci.2018.07.074.

[21] K.P. Shrestha, L. Seidel, T. Zeuch, F. Mauss, Detailed Kinetic Mechanism for the Oxidation of Ammonia Including the Formation and Reduction of Nitrogen Oxides, Energy and Fuels. 32 (2018) 10202–10217. https://doi.org/10.1021/acs.energyfuels.8b01056.

[22] J. Otomo, M. Koshi, T. Mitsumori, H. Iwasaki, K. Yamada, Chemical kinetic modeling of ammonia oxidation with improved reaction mechanism for ammonia/air and ammonia/hydrogen/air combustion, Int J Hydrogen Energy. (2018). https://doi.org/10.1016/j.ijhydene.2017.12.066.

[23] J. Jójka, R. Ślefarski, Emission Characteristics for Swirl Methane–Air Premixed Flames with Ammonia Addition, Energies (Basel). 14 (2021) 662. https://doi.org/10.3390/en14030662.

[24] T. Tomidokoro, T. Yokomori, H.G. Im, Numerical study on propagation and NO reduction behavior of laminar stratified ammonia/air flames, Combust Flame. 241 (2022) 112102. https://doi.org/10.1016/j.combustflame.2022.112102.

[25] S. Mashruk, H. Xiao, D. Pugh, M.C. Chiong, J. Runyon, B. Goktepe, A. Giles, A. Valera-Medina, Numerical Analysis on the Evolution of NH2 in Ammonia/hydrogen Swirling Flames and Detailed Sensitivity Analysis under Elevated Conditions, Combustion Science and Technology. 00 (2021) 1–28. https://doi.org/10.1080/00102202.2021.1990897.

[26] J. Atchison, JERA Targets 50% ammonia-coal co-firigin by 2030, Ammonia Energy Association. (2022).

[27] J.H. Lee, J.H. Kim, J.H. Park, O.C. Kwon, Studies on properties of laminar premixed hydrogen-added ammonia/air flames for hydrogen production, Int J Hydrogen Energy. 35 (2010) 1054–1064. https://doi.org/10.1016/j.ijhydene.2009.11.071.

[28] E.C. Okafor, M. Tsukamoto, A. Hayakawa, K.A. Somarathne, T. Kudo, T. Tsujimura, H. Kobayashi, Influence of wall heat loss on the emission characteristics of premixed ammonia-air swirling flames interacting with the combustor wall, Proceedings of the Combustion Institute. 38 (2021) 5139–5146. https://doi.org/10.1016/J.PROCI.2020.06.142.

[29] A. Alnasif, S. Mashruk, M. Kovaleva, P. Wang, A. Valera-Medina, Experimental and Numerical Analyses of Nitrogen Oxides formation in a High Ammonia-Low Hydrogen Blend using a Tangential Swirl Burner, Carbon Neutrality. (2022).

[30] S. Mashruk, M. Kovaleva, A. Alnasif, C. Tung Chong, A. Hayakawa, E.C. Okafor, A. Valera-Medina, Nitrogen oxide emissions analyses in ammonia/hydrogen/air premixed swirling flames - In Press, Energy. (2022).

[31] S. Mashruk, E.C. Okafor, M. Kovaleva, A. Alnasif, D.G. Pugh, A. Hayakawa, A. Valera-Medina, Evolution of N2O production at lean combustion condition in NH3/H2/air premixed swirling flames, Combust Flame. (2022).

[32] S.A. Alturaifi, O. Mathieu, E.L. Petersen, Shock-tube laser absorption measurements of N2O time histories during ammonia oxidation, Fuel Communications. (2022) 100050. https://doi.org/10.1016/J.JFUECO.2022.100050.

[33] C.K. Law, Combustion Physics, Cambridge University Press, Cambridge, 2010.

[34] A. Hayakawa, T. Goto, R. Mimoto, Y. Arakawa, T. Kudo, H. Kobayashi, Laminar burning velocity and Markstein length of ammonia/air premixed flames at various pressures, Fuel. 159 (2015) 98–106. https://doi.org/10.1016/j.fuel.2015.06.070.

[35] R. Kanoshima, A. Hayakawa, T. Kudo, E.C. Okafor, S. Colson, A. Ichikawa, T. Kudo, H. Kobayashi, Effects of initial mixture temperature and pressure on laminar burning velocity and Markstein length of ammonia/air premixed laminar flames, Fuel. 310 (2022) 122149. https://doi.org/10.1016/j.fuel.2021.122149.

[36] C. Lhuillier, P. Brequigny, N. Lamoureux, F. Contino, C. Mounaïm-Rousselle, Experimental investigation on laminar burning velocities of ammonia/hydrogen/air mixtures at elevated temperatures, Fuel. 263 (2020) 116653. https://doi.org/10.1016/j.fuel.2019.116653.

[37] S.-E. Zitouni, S. Mashruk, N. Mukundakumar, P. Brequigny, A. Zayoud, E. Pucci, S. Macchiavello, F. Contino, C. Mounaim-Rousselle, R. Bastiaans, A. Valera-Medina, AMMONIA BLENDED FUELS-ENERGY SOLUTIONS FOR A GREEN FUTURE, in: Gas Turbines in a Carbon-Neutral Society, 10th International Gas Turbine Conference, 2021.

[38] A. Valera-Medina, D.G. Pugh, P. Marsh, G. Bulat, P. Bowen, Preliminary study on lean premixed combustion of ammonia-hydrogen for swirling gas turbine combustors, Int J Hydrogen Energy. 42 (2017) 24495–24503.

[39] F.J. Verkamp, M.C. Hardin, J.R. Williams, Ammonia combustion properties and performance in gas-turbine burners, in: Symposium (International) on Combustion, 1967: pp. 985–992. https://doi.org/10.1016/S0082-0784(67)80225-X.

[40] D. Pugh, P. Bowen, A. Valera-Medina, A. Giles, J. Runyon, R. Marsh, Influence of steam addition and elevated ambient conditions on NOx reduction in a staged premixed swirling NH3/H2 flame, Proceedings of the Combustion Institute. 37 (2019) 5401–5409. https://doi.org/10.1016/j.proci.2018.07.091.

[41] B. Galmiche, F. Halter, F. Foucher, Effects of high pressure, high temperature and dilution on laminar burning velocities and Markstein lengths of iso-octane/air mixtures, Combust Flame. 159 (2012) 3286–3299. https://doi.org/10.1016/J.COMBUSTFLAME.2012.06.008.

[42] S. Zitouni, D. Pugh, A. Crayford, P.J. Bowen, J. Runyon, Lewis number effects on lean premixed combustion characteristics of multi-component fuel blends, Combust Flame. 238 (2022) 111932. https://doi.org/10.1016/J.COMBUSTFLAME.2021.111932.

[43] A.P. Kelley, C.K. Law, Nonlinear effects in the extraction of laminar flame speeds from expanding spherical flames, Combust Flame. 156 (2009) 1844–1851. https://doi.org/10.1016/j.combustflame.2009.04.004.

[44] A. Valera-Medina, M. Gutesa, H. Xiao, D. Pugh, A. Giles, B. Goktepe, R. Marsh, P. Bowen, Premixed ammonia/hydrogen swirl combustion under rich fuel conditions for gas turbines operation, Int J Hydrogen Energy. 44 (2019) 8615–8626. https://doi.org/10.1016/j.ijhydene.2019.02.041.

[45] A. Gaydon, The spectroscopy of flames, 2012.

[46] K. Ohashi, T. Kasai, D.C. Che, K. Kuwata, Alignment dependence of the amidogen chemiluminescence in the reaction of argon(3P) atoms with the aligned ammonia molecules, Journal of Physical Chemistry. 93 (2002) 5484–5487. https://doi.org/10.1021/J100351A033.

[47] G.L. Schott, L.S. Blair, J.D.M. Jr., Exploratory shock-wave study of thermal nitrogen trifluoride decomposition and reactions of nitrogen trifluoride and dinitrogen tetrafluoride with hydrogen, Journal of Physical Chemistry. 77 (2002) 2823–2830. https://doi.org/10.1021/J100642A001.

[48] T.R. Roose, R.K. Hanson, C.H. Kruger, A shock tube study of the decomposition of no in the presence of NH3, Symposium (International) on Combustion. 18 (1981) 853–862. https://doi.org/10.1016/S0082-0784(81)80089-6.

[49] Y. Yi, R. Zhang, L. Wang, J. Yan, J. Zhang, H. Guo, Plasma-Triggered CH4/NH3 Coupling Reaction for Direct Synthesis of Liquid Nitrogen-Containing Organic Chemicals, ACS Omega. (2017). https://doi.org/10.1021/acsomega.7b01060.

[50] S. Mashruk, NO Formation Analysis using Chemical Reactor Modelling and LIF Measurements on Industrial Swirl Flames - PhD Thesis, Cardiff University, 2020. https://doi.org/10.13140/RG.2.2.28297.06246/1.

[51] M.J. Bedard, T.L. Fuller, S. Sardeshmukh, W.E. Anderson, Chemiluminescence as a diagnostic in studying combustion instability in a practical combustor, Combust Flame. 213 (2020) 211–225. https://doi.org/10.1016/J.COMBUSTFLAME.2019.11.039.

[52] S. Mashruk, M.O. Vigueras-Zuniga, M.E. Tejeda-del-Cueto, H. Xiao, C. Yu, U. Maas, A. Valera-Medina, Combustion features of CH4/NH3/H2 ternary blends, Int J Hydrogen Energy. (2022). https://doi.org/10.1016/J.IJHYDENE.2022.03.254.

[53] D. Pugh, J. Runyon, P. Bowen, A. Giles, A. Valera-Medina, R. Marsh, B. Goktepe, S. Hewlett, An investigation of ammonia primary flame combustor concepts for emissions reduction with OH*, NH2* and NH* chemiluminescence at elevated conditions, Proceedings of the Combustion Institute. 38 (2021) 6451–6459. https://doi.org/10.1016/j.proci.2020.06.310.

[54] C.R. Shaddix, A new method to compute the proper radiant heat transfer correction of bare-wire thermocouple measurements, in: 10th U.S. National Combustion Meeting, 2017.

[55] S. Mashruk, H. Xiao, A. Valera-Medina, Rich-Quench-Lean model comparison for the clean use of humidified ammonia/hydrogen combustion systems, Int J Hydrogen Energy. 46 (2020) 4472–4484. https://doi.org/10.1016/j.ijhydene.2020.10.204.

[56] S. Mashruk, E.C. Okafor, M. Kovaleva, A. Alnasif, D. Pugh, A. Hayakawa, A. Valera-Medina, Evolution of N2O production at lean combustion condition in NH3/H2/air premixed swirling flames, Combust Flame. 244 (2022) 112299. https://doi.org/10.1016/J.COMBUSTFLAME.2022.112299.

[57] S. Mashruk, H. Xiao, D. Pugh, M.C. Chiong, J. Runyon, B. Goktepe, A. Giles, A. Valera-Medina, Numerical Analysis on the Evolution of NH2 in Ammonia/hydrogen Swirling Flames and Detailed Sensitivity Analysis under Elevated Conditions, Combustion Science and Technology. 00 (2021) 1–28. https://doi.org/10.1080/00102202.2021.1990897.

[58] S. Mashruk, E.C. Okafor, M. Kovaleva, A. Alnasif, D.G. Pugh, A. Hayakawa, A. Valera-Medina, Evolution of N2O production at lean combustion condition in NH3/H2/air premixed swirling flames, Combust Flame. (2022).

[59] Alessandro Stagni, Carlo Cavallotti, Suphaporn Arunthanayothin, Yu Song, Olivier Herbinet, Frédérique Battin-Leclerc, Tiziano Faravelli, An experimental, theoretical and kinetic-modeling study of the gas-phase oxidation of ammonia, React Chem Eng. 5 (2020) 696–711. https://doi.org/10.1039/C9RE00429G.

[60] G.J. Gotama, A. Hayakawa, E.C. Okafor, R. Kanoshima, M. Hayashi, T. Kudo, H. Kobayashi, Measurement of the laminar burning velocity and kinetics study of the importance of the hydrogen recovery mechanism of ammonia/hydrogen/air premixed flames, Combust Flame. (2021).

[61] P. Glarborg, J.A. Miller, B. Ruscic, S.J. Klippenstein, Modeling nitrogen chemistry in combustion, Prog Energy Combust Sci. 67 (2018) 31–68. https://doi.org/10.1016/j.pecs.2018.01.002.

[62] A. Alnasif, S. Mashruk, M. Kovaleva, P. Wang, A. Valera-Medina, Experimental and Numerical Analyses of Nitrogen Oxides formation in a High Ammonia-Low Hydrogen Blend using a Tangential Swirl Burner, Carbon Neutrality. (2022).

[63] N. Syred, C. Wong, V. Rodriquez-Martinez, J. Dawson, R. Kelso, Characterisation of the occurrence of the precessing vortex core in partially premixed and non-premixed swirling flow, in: Proceedings of The12th International Symposium on the Applications of Laser Techniques to Fluid Mechanics, Lisbon, 2004.

[64] A. Valera-Medina, N. Syred, A. Griffiths, Visualisation of isothermal large coherent structures in a swirl burner, Combust Flame. 156 (2009). https://doi.org/10.1016/j.combustflame.2009.06.014.

[65] S. Mashruk, M.O. Vigueras-Zuniga, M.E. Tejeda-del-Cueto, H. Xiao, C. Yu, U. Maas, A. Valera-Medina, Combustion features of CH4/NH3/H2 ternary blends, Int J Hydrogen Energy. (2022). https://doi.org/10.1016/J.IJHYDENE.2022.03.254.

[66] R. d'Agostino, F. Cramarossa, S. De Benedictis, G. Ferraro, Kinetic and spectroscopic analysis of NH3 decomposition under R.F. Plasma at moderate pressures, Plasma Chemistry and Plasma Processing. 1 (1981) 19–35. https://doi.org/10.1007/BF00566373.

[67] J. Ballester, T. García-Armingol, Diagnostic techniques for the monitoring and control of practical flames, Prog Energy Combust Sci. 36 (2010) 375–411. https://doi.org/10.1016/j.pecs.2009.11.005.

[68] S.L. Sheehe, S.I. Jackson, Spatial distribution of spectrally emitting species in a nitromethane–air diffusion flame and comparison with kinetic models, Combust Flame. 213 (2020) 184–193. https://doi.org/10.1016/J.COMBUSTFLAME.2019.10.026.

[69] M.V. Manna, P. Sabia, G. Sorrentino, T. Viola, R. Ragucci, M. de Joannon, New insight into NH3-H2 mutual inhibiting effects and dynamic regimes at low-intermediate temperatures, Combust Flame. (2022) 111957. https://doi.org/10.1016/J.COMBUSTFLAME.2021.111957.

[70] M.O. Vigueras-Zúñiga, M.E. Tejeda-Del-cueto, S. Mashruk, M. Kovaleva, C.L. Ordóñez-Romero, A. Valera-Medina, Methane/Ammonia Radical Formation during High Temperature Reactions in Swirl Burners, Energies 2021, Vol. 14, Page 6624. 14 (2021) 6624. https://doi.org/10.3390/EN14206624.

[71] K.D.K.A. Somarathne, S. Hatakeyama, A. Hayakawa, H. Kobayashi, Numerical study of a low emission gas turbine like combustor for turbulent ammonia/air premixed swirl flames with a secondary air injection at high pressure, Int J Hydrogen Energy. 42 (2017) 27388–27399. https://doi.org/10.1016/j.ijhydene.2017.09.089.

[72] E.C. Okafor, K.D.K.A. Somarathne, R. Ratthanan, A. Hayakawa, T. Kudo, O. Kurata, N. Iki, T. Tsujimura, H. Furutani, H. Kobayashi, Control of NOx and other emissions in micro gas turbine combustors fuelled with mixtures of methane and ammonia, Combust Flame. 211 (2020) 406–416. https://doi.org/10.1016/j.combustflame.2019.10.012.

[73] E.C. Okafor, K.D.K.A. Somarathne, A. Hayakawa, T. Kudo, O. Kurata, N. Iki, H. Kobayashi, Towards the development of an efficient low-NOx ammonia combustor for a micro gas turbine, Proceedings of the Combustion Institute. 37 (2019) 4597–4606. https://doi.org/10.1016/j.proci.2018.07.083.

[74] M. Guteša Božo, S. Mashruk, S. Zitouni, A. Valera-Medina, Humidified ammonia/hydrogen RQL combustion in a trigeneration gas turbine cycle, Energy Convers Manag. 227 (2021) 113625. https://doi.org/10.1016/j.enconman.2020.113625.

[75] P. Sabia, M.V. Manna, R. Ragucci, M. de Joannon, Mutual inhibition effect of hydrogen and ammonia in oxidation processes and the role of ammonia as “strong” collider in third-molecular reactions, Int J Hydrogen Energy. 45 (2020) 32113–32127. https://doi.org/10.1016/j.ijhydene.2020.08.218.

[76] S. Mashruk, M. Kovaleva, A. Alnasif, C.T. Chong, A. Hayakawa, E.C. Okafor, A. Valera-Medina, Nitrogen oxide emissions analyses in ammonia/hydrogen/air premixed swirling flames, Energy. 260 (2022) 125183. https://doi.org/10.1016/J.ENERGY.2022.125183.